ORIGINAL RESEARCH

Transferrin-Modified Osthole PEGylated Liposomes Travel the Blood-Brain Barrier and Mitigate Alzheimer's Disease-Related Pathology in APP/PS-1 Mice

Liang Kong[1]
Xue-tao Li[1]
Ying-nan Ni[1]
Hong-he Xiao[1]
Ying-jia Yao[2]
Yuan-yuan Wang[3]
Rui-jun Ju[4]
Hong-yan Li [ID][1]
Jing-jing Liu[1]
Min Fu[1]
Yu-tong Wu[1]
Jing-xian Yang[1]
Lan Cheng[1]

[1]School of Pharmacy, Liaoning University of Traditional Chinese Medicine, Dalian 116600, People's Republic of China; [2]College of Life and Health Sciences, Northeastern University, Shenyang 110819, People's Republic of China; [3]Department of Pharmacy, The Affiliated Zhongshan Hospital of Dalian University, Dalian, Liaoning 116001, People's Republic of China; [4]Department of Pharmaceutical Engineering, Beijing Institute of Petrochemical Technology, Beijing 102617, People's Republic of China

Correspondence: Jing-xian Yang; Lan Cheng
Email jingxianyang0520@163.com; sychenglan@163.com

Introduction: Osthole (Ost) is a coumarin compound that strengthens hippocampal neurons and neural stem cells against Aβ oligomer-induced neurotoxicity in mice, and is a potential drug for the treatment of Alzheimer's disease (AD). However, the effectiveness of the drug is limited by its solubility and bioavailability, as well as by the low permeability of the blood-brain barrier (BBB). In this study, a kind of transferrin-modified Ost liposomes (Tf-Ost-Lip) was constructed, which could improve the bioavailability and enhance brain targeting.

Methods: Tf-Ost-Lip was prepared by thin-film hydration method. The ability of liposomal formulations to translocate across BBB was investigated using in vitro BBB model. And the protective effect of Tf-Ost-Lip was evaluated in APP-SH-SY5Y cells. In addition, we performed pharmacokinetics study and brain tissue distribution analysis of liposomal formulations in vivo. We also observed the neuroprotective effect of the varying formulations in APP/PS-1 mice.

Results: In vitro studies reveal that Tf-Ost-Lip could increase the intracellular uptake of hCMEC/D3 cells and APP-SH-SY5Y cells, and increase the drug concentration across the BBB. Additionally, Tf-Ost-Lip was found to exert a protective effect on APP-SH-SY5Y cells. In vivo studies of pharmacokinetics and the Ost distribution in brain tissue indicate that Tf-Ost-Lip prolonged the cycle time in mice and increased the accumulation of Ost in the brain. Furthermore, Tf-Ost-Lip was also found to enhance the effect of Ost on the alleviation of Alzheimer's disease-related pathology.

Conclusion: Transferrin-modified liposomes for delivery of Ost has great potential for AD treatment.

Keywords: transferrin, osthole, liposomes, blood-brain barrier, Alzheimer's disease

Introduction

Alzheimer's disease (AD) is a devastating neurodegenerative disease, the clinical symptoms of which are cognitive and memory dysfunction accompanied by mental and behavioral disorders.[1] It affects approximately 50 million people worldwide, and, according to the 2018 World Alzheimer Report, the number of patients will increase exponentially every 20 years.[2] The pathological features of AD include β-amyloid polypeptide (Aβ) deposition, hyperphosphorylated tau aggregation, synapses and neuronal loss, and neuroinflammation, among others.[3] In recent years, listed drugs have been found to only alleviate the disease, and there are no

safe and effective drugs to prevent or cure AD. Based on the targeted Aβ, researchers have sought to find effective drugs to inhibit Aβ protein production or aggregation, or to promote its clearance; however, these drugs have failed to reverse AD or delay progression.[4] In particular, the failure of monoclonal drugs targeting BACE1 inhibitors (solane-zumab and bapineuzumab) in clinical trials challenged the reliability of Aβ as a therapeutic target; thus, it is important to find new and effective therapeutic targets.[5] In addition to finding new potential targets for the treatment of AD, it is also important to develop a strategy to help drugs cross the blood-brain barrier (BBB) and achieve intracranial drug delivery.[6] The presence of the BBB greatly hinders the accumulation of drugs into the brain, resulting in poor efficacy. Only high fat-soluble substances with a molecular weight of less than 400 Da can pass through the BBB, and only about 2% of drug molecules meet these requirements.[7] Therefore, the development of drug delivery systems that could transport drugs across the BBB is an urgent and necessary task. Liposomes, nano-particles, polymer micelles, and vesicles are widely used in this field.[8–11]

Liposomes, as nanoscale drug carriers, are a promising drug delivery system that can encapsulate both hydrophilic and hydrophobic drugs; hydrophilic drugs are encapsu-lated in an aqueous core, and lipophilic drugs are encap-sulated in a hydrophobic region of the lipid bilayer. The lipid bilayer of liposomes is composed of phospholipids and cholesterol, and are very similar to cell membranes.[12] In addition, liposomes offer numerous advantages, includ-ing targeting capability, long-term efficacy, improved drug stability, lowered drug toxicity, and increased circulation time. Liposomes are also capable of achieving targeting by modifying proteins, antibodies, aptamers, or polypeptides.[13] These properties of liposomes have attracted interest in their development as possible new and effective treatments for AD.[14] Transferrin (Tf) is a ligand that is commonly used for drug-targeted BBBs, and can effectively promote the accumulation of drugs in the brain.[15] Tf binds to the specific transferrin receptor (TfR) on the BBB and crosses the BBB via receptor-mediated endocytosis, thereby allowing for drug accumu-lation in the brain to be improved.[16] Research has shown that liposomes modified with Tf can penetrate the BBB and subsequently target neural cells.[17,18]

Osthole, a natural coumarin derivative (7-methoxy-8-isopen-tenoxycoumarin, Ost, $C_{15}O_{16}O_3$, 244.39 Da), has been isolated from some medicinal plants, such as *Radix Angelicae pubescentis, Cnidium monnieri, Angelica pubescens*, and *Peucedanum ostruthium*. The compound has attracted much attention due to its broad pharmacological effects, including its anti-inflammatory, anti-apoptotic, anti-oxidative stress, and neurotrophic fac-tor-like properties.[19,20] Current research indicates that Ost has an improved effect on degenerative diseases of the central nervous system, such as Alzheimer's disease.[21–23] Ost can partially pass through the BBB as a small fat-soluble molecule, but its neuroprotective efficacy is lim-ited by its poor solubility, poor stability, poor brain target-ing, and low bioavailability.[24] Liposomes, nanoparticles, microspheres, and other nano-drug carriers are considered to be effective methods for the improvement of the bioa-vailability of Ost.

The neuroprotective effects of Tf-modified targeted liposomes with the incorporation of Ost are investigated in the present study (Figure 1). Tf is modified on the surfaces of the targeted liposomes to increase the effi-ciency of BBB transmission, and Ost is encapsulated in the lipid bilayer membrane as a therapeutic drug. The characteristics of the liposomes, cellular uptake, ability to cross a model BBB, pharmacokinetics in plasma, drug content in the brain, and its improvement on model AD both in vitro and in vivo are systematically examined.

Materials and Methods
Materials, Cells and Animals
Egg yolk phosphatidylcholine (EPC), cholesterol (Chol), and 1.2-distearoyl-sn-glycero-3-phosphoethanolamine-N [carboxy (polyethylene glycol)-2000] (DSPE-PEG$_{2000}$-MAL) were obtained from the Avanti Polar Lipids, Inc. (Purity>99%, Alabaster, AL, USA). Polyethylene glycol-distearoyl phosphatidylethanolamine (DSPE-PEG$_{2000}$) was purchased from the NOF Corporation (Purity>99.9%, Tokyo, Japan). Ost was obtained from the Chengdu Derick Biotechnology Co., Ltd. (Purity>99.8%, Chengdu, China). Holo-transferin and Rhodamine B (RhB) was ordered from Sigma-Aldrich (Purity>99.9%, St. Louis, MO, USA). The bicinchoninic acid (BCA) kit was pro-vided by the Beyotime Biotechnology Co., Ltd. (Jiangsu, China). 4′,6-diamidino-2-phenylindole (DAPI) and 1.1-dioctadecyl-3,3,3,3- tetramethylindotricarbocyanine iodide (DiR) were obtained from the Kaiji Biological Technology Development Co., Ltd. (Purity>99%, Nanjing, China). The lentiviral vectors with APP (KM670/671NL), pLP1, pLP2 and pLP/VSVG plasmids
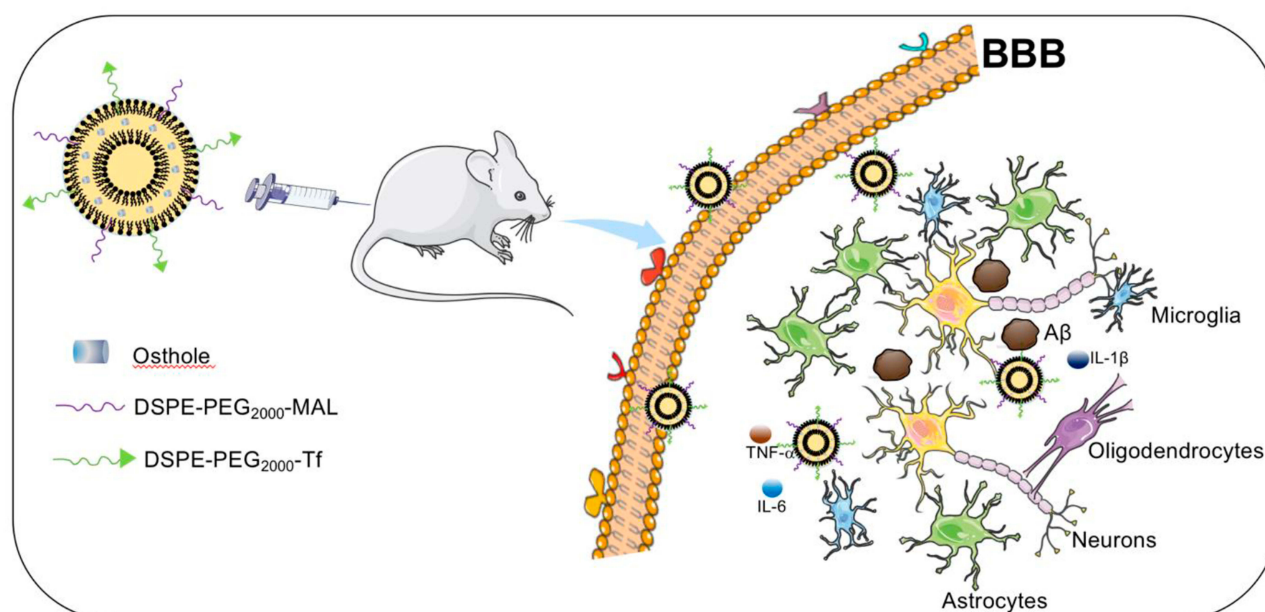
Figure 1 Schematic illustration of strategy for improving AD-related pathology by Tf-modified osthole liposomes.

were purchased from GeneCopoeia Biotechnology Co. Ltd (Guangzhou, China). Lipofectamine TM2000 according to the manufacturer's was obtained from Invitrogen Corporation (Carlsbad, USA). The Cell Counting Kit-8 (CCK-8) was supplied by the Meilun Biotechnology Co., Ltd. (Dalian, China). Bax, Bcl-2, Cleaved-caspase-3, GFAP antibodies and HRP-labelled secondary antibodies were purchased from Biosynthesis Biotechnology Co., Ltd. (Beijing, China). $A\beta_{1-42}$, NeuN antibodies were ordered from Abcam Co., Ltd. (Cambridge, MA, USA). Iba-1 antibody was obtained from FUJIFILM Wako Pure Chemical Corporation (Osaka, Japan). Fluorescein isothiocyanate (FITC)- or Cy3-conjugated secondary antibodies were offered from Jackson ImmunoResearch Lab, (West Grove, PA, USA). All other reagents used were of analytical grade.

Human neuroblastoma cells (SH-SY5Y), human embryonic kidney (HEK293T) and human brain endothelial cells (hCMEC/D3) were purchased from the Institute of Basic Medical Science, Chinese Academy of Medical Science (Beijing, China). SH-SY5Y and HEK293T were cultured in DMEM/F12 culture medium supplemented with 10% fetal bovine serum (FBS) (EallBio, Beijing, China), 1% penicillin-streptomycin (Meilun, Dalian, China). HCMEC/D3 was maintained in ECM medium (SclenCell, Carlsbad, USA) supplemented with 5% FBS, 1% penicillin-streptomycin, 1.4 μM hydrocortisone, 5 μg/mL ascorbic acid, 1/100 chemically defined lipid

concentrate, 10 mM HEPES and 1 ng/mL basic FGF (bFGF). The cells were cultured at 37 °C in a humidified atmosphere of 95% air and 5% CO_2. 7-month-old APP/PS-1 double transgenic (Tg) mice were purchased from the Model Animal Resource Information Platform (Nanjing, China). The same age C57BL/6 mice and SD rats were purchased from Liaoning Changsheng Biological Co., Ltd (Liaoning, China). All procedures were performed according to the guidelines of Liaoning University of Traditional Chinese Medicine Institutional Animal Care and Use Committee, and this research was approved by Liaoning University of Traditional Chinese Medicine Institutional Animal Care and Use Committee (IACUC2018018).

Preparation of Liposomes

Tf-modified Ost liposomes (Tf-Ost-Lip) were prepared using thin-film hydration. First, transferrin was dissolved at a concentration of 1 mg/mL and thiolated with Traut's reagent in HEPES buffer (10 mM HEPES with 150 mM NaCl, pH = 8.5); the molar ratio of Traut's reagent to transferrin was 50:1. Non-reacted Traut's reagent was then removed with an Amicon Ultra-0.5 filter (MWCO: 30 kDa, Millipore), and the thiolated transferrin solution was concentrated. Ellman's reagent was employed to test the amount of sulfhydryl groups conjugated to transferrin.[25] Lipid compositions of EPC/Chol/DSPE-PEG$_{2000}$ (100:40:3.8, molar ratio), EPC/Chol/DSPE-PEG$_{2000}$/Ost (100:40:3.8:17.3, molar ratio), and EPC/Chol/DSPE-

PEG_{2000}/DSPE-PEG_{2000}-MAL/Ost (100:40:3.8:1.5:17.3, molar ratio) were respectively used for the preparation of blank liposomes, Ost liposomes (Ost-Lip), and Tf-modified Ost liposomes (Tf-Ost-Lip). Then, EPC, Chol, DSPE-PEG_{2000}, DSPE-PEG_{2000}-MAL, and Ost were dissolved in methyl alcohol in a pear-shaped bottle and dried via a rotary evaporator at 37 °C to obtain a thin film, and the thin film was hydrated with 5 mL of Tris base solution (pH = 10.0) via sonication in a water bath. The suspensions were then sonicated in an ice bath with a probe sonicator for 10 min at 200 W (JY92-IIN, Xinzhi Biotechnology Co., Ltd., Ningbo, China). Subsequently, the samples were thrice extruded through polycarbonate membranes with 200 nm pores, thus completing the preparation of the Ost liposomes. The thiolated transferrin was then incubated with liposomes overnight under a nitrogen flow at room temperature, and the thiolated transferrin to maleimide ratio was 1:2 (molar ratio), thus completing the preparation of the Tf-modified Ost liposomes. In addition, Ost liposomes and blank liposomes were prepared by the same processes as described previously, except for the addition of thiolated transferrin or Ost, respectively. Liposomes loaded with DiR or RhB were also prepared according to this procedure, but the drug was replaced with a fluorescent probe (EPC: DiR, 200:1, w/w; EPC: RhB = 100:7, molar ratio).

Characterization of Liposomes

The particle size, polydispersity index, and zeta potential values of all liposomes were determined using dynamic light scattering with a Zetasizer Nano ZS90 instrument (Malvern, UK). The morphologies of the liposomes were observed using transmission electron microscopy (TEM, JEM-1200EX; JEOL, Tokyo, Japan) and atomic force microscopy (Cypher AFM, Asylum Research Inc., Santa Barbara, CA, USA). The Ost content was measured using a high-performance liquid chromatography system (HPLC) with an ultraviolet detector (Shimadzu LC-2010AHT). The un-encapsulated drug was separated by ultracentrifugation (12,000 rpm, 30 min) (TGL-20M, Xiangyi Centrifuge Instrument Co., Ltd., Changsha, China). The encapsulation efficiency (EE) was calculated using the following equation: $EE\% = (W_{encapsulated}/W_{total}) \times 100\%$, where $W_{encapsulated}$ and W_{total} represent the amount of drugs in the liposomes and the total amount of drugs, respectively.[26] The drug loading (DL%) of Ost-loaded liposomes was calculated using the follow equation: $DL\% = (W_{loaded\ drug}/W_{Total\ amount\ of\ lipids}) \times 100\%$. According to the authors' previous reports, the release

behaviors of the Ost-Lip and Tf-Ost-Lip were assessed by dialysis in vitro. In short, equal volumes of Ost-Lip, Tf-Ost-Lip, and Ost solution (1 mL) were placed in a dialysis bag (MW cut-off, 8000–14,000 Da). The dialysis bag was immersed in 30 mL PBS solution containing 10% FBS, and oscillated by gentle shaking (100 rpm) at 37 °C. At predetermined time intervals (6, 12, 24, 36, 48, and 72 h), 500 μL of the release medium was removed and replaced by the same volume of fresh PBS. The Ost content in the release medium was determined by HPLC.[25] In addition, the binding efficiency of Tf on the liposomes was determined by a BCA kit, and the calculation formula is as follows: binding efficiency % = ($W_{binding\ protein}$/$W_{total\ protein}$) × 100%.[25] The liposome storage stability was also analyzed. Briefly, Ost-Lip and Tf-Ost-Lip were transferred to a sealed brown glass bottle (n = 3) and stored at room temperature (25 °C) and at 4 °C for 30 d. The particle size, zeta potential, and encapsulation efficiency of the liposomes were measured at predetermined time intervals (0, 10, 20, and 30 days) during storage.

Cell Transfection

SH-SY5Y and HEK293T were cultured in F12 culture medium supplemented with 10% FBS, 100 U/mL penicillin, and 100 μg/mL streptomycin at 37 °C in a humidified atmosphere of 95% air and 5% CO_2. Then, the lentiviral vectors with APP-GFP or GFP, along with packaging plasmids pLP1, pLP2, and pLP/VSV-G, were fused into HEK293T with Lipofectamine 2000. Green fluorescence was observed in both groups under a fluorescence microscope within 24 h. Supernatants containing lentivirus were collected from the HEK293T at 36 and 72 h after transfection, centrifuged at 3000 rpm for 30 min to remove cellular debris, and sterilized by filtration (0.22 μm). Supernatants were centrifuged at 6000 rpm for 1 h with a cutoff of 100 kDa to obtain concentrated virus titers. SH-SY5Y was infected with concentrated viral supernatant. The overexpression of APP was confirmed by Western blot and fluorescence microscopy.[3]

Cellular Uptake

Flow cytometry was employed to study the uptake of fluorescently-labeled RhB liposomes (RhB-Lip) and Tf-modified RhB liposomes (Tf-RhB-Lip) in hCMEC/D3 cells.[27] hCMEC/D3 cells were cultured (1×10^6 cells) in 6-well plates and were allowed to adhere for 24 h. Then, RhB-Lip and Tf-RhB-Lip were added into the cultured medium and blank liposomes were used as blank controls.

The final concentration of RhB was 10 μM. Cells were incubated for 2 h, and cells treated with Tf-modified RhB liposomes were incubated for different amounts of time (1, 2, and 3 h). Subsequently, cells were washed with PBS to remove excess drugs, trypsinized, harvested, and centrifuged at 1500 rpm for 3 min. Cells were resuspended in 500 μL PBS, and the fluorescence intensities of the samples were quantitatively assessed via flow cytometry (BD Biosciences, Franklin Lakes, NJ).

The cellular uptake of RhB-Lip or Tf-RhB-Lip in hCMEC/D3 cells was further verified using fluorescence microscopy. Briefly, hCMEC/D3 cells were incubated with RhB-Lip and Tf-RhB-Lip at a 10-μM final concentration of RhB, and blank liposomes was used as a blank control. After 2 hours of incubation, the cells were washed with PBS, fixed with 4% paraformaldehyde for 15 min at room temperature (RT), and the nuclei were then stained with DAPI for 15 min. Finally, fluorescence images of hCMEC/D3 cells were observed by a fluorescence microscope (Nikon Eclipse E800, Nikon, Tokyo).

BBB Model
The hCMEC/D3/SH-SY5Y cell co-culture BBB model was established as previously reported.[28] In brief, hCMEC/D3 cells (1×10^5 cells) were seeded into a transwell chamber in a 24-well plate (Corning, NY, USA). SH-SY5Y cells were seeded (2×10^3 cells/compartment) in the basolateral compartment of the insert. Cells were allowed to culture for 7 days. The culture medium was changed every 2 days, and the monolayers were evaluated for the following experiments to check the integrity of the BBB model. Sodium fluorescein (Na-FLU) permeability and TEER were measured by a Millicell ERS-2 volt-ohm meter (Millipore Corp.) and an STX01 chopstick-style electrode (Millipore).

Transport Across the BBB Model
After an in vitro BBB model was established, Ost-Lip and Tf-Ost-Lip at concentrations of 1 mM were applied to the apical compartment of the BBB model, and D-Hank's solution was used as a transport medium. The TEER value was measured during the experiment. After 2, 3, and 4 h of treatment, a 200 μL sample was taken from the basolateral compartment and immediately replaced with 200 μL of D-Hank's solution. The drug content in the basolateral compartment was determined using HPLC.[15]

The Protective Effect of Tf-Ost-Lip in vitro
APP-transfected SH-SY5Y cells (APP-SH-SY5Y cells) were used to evaluate the protective effect of Ost-loaded liposomes. APP-SH-SY5Y cells were treated with Ost-Lip and Tf-Ost-Lip, and the final concentration of Ost was 100 μM. After incubation for 24 h, the viability of cells was measured by Cell Counting Kit-8 (CCK-8) assays, $A\beta_{42}$ expression was detected by immunofluorescence staining, and the apoptotic rate was detected by flow cytometry according to the manufacturer's instruction.

Pharmacokinetics Study
Healthy SD rats weighing approximately 200 g were randomly divided into three groups (n=6). The varying Ost formulations, namely the free Ost solution, Ost-Lip, and Tf-Ost-Lip, were injected into the rats through the tail vein at a dose of 10 mg/kg. Blood samples (0.5 mL) were collected in heparinized tubes from the orbital vein at predetermined time points, namely 0.083, 0.25, 0.5, 0.75, 1, 1.5, 2, 4, 6, 9, 12, 24, and 48 h. The concentration of Ost in the blood was monitored using the HPLC method, the parameters of which were as follows: column, Diamonsil C18 (5 μm, 250 × 4.6 mm); mobile phase, methanol and water (80:20, v/v); flow rate, 1.0 mL/min; injection volume, 20 μL; internal standard, paeonol; detection wavelength, 322 nm; column temperature, 30 °C. Data were analyzed using the pharmacokinetic software Kinetica, and the pharmacokinetic parameters were calculated based on a two-compartment pharmacokinetic model fitted with a first-order absorption elimination rate constant.

Ost Distribution in the Brains of APP/PS-1 Mice
APP/PS-1 mice weighing about 30 g were randomly divided into three groups. Three different Ost formulations, namely the free Ost solution, Ost-Lip, and Tf-Ost-Lip, were injected into the mice via the tail vein at a dose of 10 mg/kg. At 0.5, 2, 4, 6, 12, and 24 h after injection, the mice in each group were sacrificed and brain tissue was dissected, washed with PBS to wash away the blood attached to the organs, and weighed (n=6). The concentration of the drug in the brain tissue was determined using HPLC as described above. The results were expressed as the drug concentration in the brain and the percentage of the injected dose/gram of tissue (%ID/g).

Imaging in APP/PS-1 Mice

APP/PS-1 mice were used to evaluate the distribution of Tf-modified liposomes in vivo. First, normal saline, free DiR, DiR liposomes, and Tf-modified DiR (2 μg DiR per mouse) were injected through the tail vein (n = 3). Subsequently, the mice were anesthetized with isoflurane, and fluorescence images and normal images of the mice were captured at 1, 3, 6, 12, and 24 h using an in-vivo fluorescence imaging system (Carestream, FX Pro, USA).

The Protective Effect of Tf-Ost-Lip in vivo

Forty APP/PS-1 mice were randomly divided into four groups, and wild-type (WT) littermate mice of the same age served as controls. All mice were separated into five groups (n=6), namely the control group, APP group, Ost group, Ost-Lip group, and Tf-Ost-Lip group. The Ost-treated APP/PS-1 mice, Ost-Lip-treated APP/PS-1 mice, and Ost-Lip-treated APP/PS-1 mice were intraperitoneally injected with the Ost solution, Ost-Lip, and Tf-Ost-Lip, respectively (all 10 mg/kg) every day for 30 days. The mice in the control and model groups were treated with PBS. At the end of the treatment, each group of mice was sacrificed to evaluate the therapeutic effects. The levels of IL-6, TNF-α, IL-1β, SOD activity, and MDA content were determined according to the manufacturer's instructions to evaluate the inflammatory response and oxidative stress of APP/PS-1 mice after treatment with the varying formulations. In addition, immunofluorescence/immunocytochemistry analyses were conducted to detect the expressions of Bax, Bcl-2, cleaved caspase-3, Iba-1, and $A\beta_{1-42}$. Transmission electron microscopy was also performed to detect the synaptic density in the hippocampi of the mice, and $A\beta_{1-42}$ protein expression was tested by Western blot analysis.

Morris Water Maze

After 25 days of treatment with the varying formulations, the Morris water maze (MWM) test was implemented as described in existing literature to evaluate the learning and memory capacity of the mice.[29,30] The apparatus consisted of a circular pool (120 cm in diameter and 60 cm in height) and a black inner wall, which was subdivided into four equal quadrants and filled with water (25 °C) to a depth of 30 cm. The escape platform (10 cm in diameter) was placed in a quadrant (target quadrant) and submerged about 1 cm below the surface of the water. The escape latency of the mice was observed for five consecutive days in the four quadrants, and the time at which the mice found the hidden platform was recorded. If the mice were unable to reach the platform within 60 s, they were guided to the platform where they were held for 10 s. After five days of training, the platform was removed and a spatial probe test was conducted, the mice were placed at the start, and their behavior was observed for 60 seconds. All images and data were recorded by an automated tracking system (Chengdu TME Technology Co, Ltd., Chengdu, China).

Nest Building

Nest building assays were modified to determine defects in the social behavior of APP/PS-1 mice and potential changes after treatment. Mice were housed individually in clean plastic cages containing 1 cm of wood chip pads for at least 24 hours. One hour prior to the onset of the dark period, a cotton pad torn into 5 x 5 cm square pieces was provided on one side of the cage. On the morning of the third day, the nests of the mice were observed and photographed, and the nesting score of each mouse was evaluated according to previous research.[31]

Statistical Analysis

Statistical analysis was performed by using GraphPad Prism 6.0 software, and the data were expressed as the mean ± standard deviation (mean ± SD). Differences between groups were assessed by one-way analysis of variance (ANOVA). Post-hoc multiple comparisons were performed with the Student-Newman-Keuls test. $P < 0.05$ was considered to be statistically significant.

Results and Discussion

AD is an incurable multifactorial neurodegenerative disease characterized by Aβ deposition and tau hyperphosphorylation leading to neuronal loss and changes in different cellular pathways.[32] Although the past decade has witnessed enormous breakthroughs in the pathogenesis and treatment of AD in the laboratory, this information has been rarely translated into effective clinical treatments. One of the major limitations of new active molecules synthesized or discovered for AD is their poor stability and poor bioavailability, and especially their inability to cross the BBB.[33,34] Therefore, Tf-modified liposomes capable of penetrating the BBB were developed in this study. Additionally, we also encapsulated Ost, an effective Chinese medicine monomer for Alzheimer's disease in our previous study.[19–23] It was hypothesized that Tf mediates the transport of Ost-Lip through the BBB via TfRs located on the surfaces of brain

capillary endothelial cells, thereby increasing the accumulation of Ost in the brain. Several reports have indicated that Tf-modified liposomes could be used to transport drugs across the BBB. For instance, Chen et al demonstrated that Tf-modified liposomes promote α-M penetration through the BBB and increase drug accumulation in the brain, thereby significantly increasing bioavailability.[35] Sonali et al reported that Tf-modified liposomes may be a promising carrier for brain theranostics due to their nano-sized delivery and permeability, which contribute to the improved and prolonged brain targeting of docetaxel and quantum dots.[36] Lakkadwala et al also revealed a dual-functionalized liposome delivery system with Tf and cell-penetrating peptide-pectin (Pen), which enhances the anti-glioma efficacy of doxorubicin and erlotinib.[37]

Characterization of the Liposomes

Physical properties including the particle size, polydispersity index (PDI), zeta potential, encapsulation efficiency, drug loading capacity, and Tf grafting rate are exhibited in Table 1. The encapsulation efficiencies of Ost were greater than 90% for the Ost liposomes and Tf-modified Ost liposomes. The drug loading capacities of these liposomes were found to be $3.91 \pm 0.076\%$ and $3.71 \pm 0.038\%$, respectively. The particle sizes of the blank liposomes, Tf-modified blank liposomes, Ost liposomes, and Tf-modified Ost liposomes were found to be approximately 100 nm with a narrow polydispersity index (≤0.20) and a normal distribution, indicating that the particle size distribution of Tf-Ost-Lip is uniform (Figure S1). Table 1 also reveals that Tf surface conjugation increased the overall liposome size by about 10 nm. The molecular weight of transferrin is only 79,500, and it is therefore a small-molecule peptide. After modification of the nanoparticle surface, the particle size only increased slightly. This is consistent with the results of previous studies.[36,38,39] None of the liposomes exhibited any significant alteration after Tf decoration, indicating

that the stabilities of the liposomes were not influenced by Tf. The zeta potential values were found to be -3.48 ± 0.23 mV for Ost liposomes and -6.95 ± 0.51 mV for Tf-modified Ost liposomes. The zeta potential represents the charge on the particle surface. The addition of fat-soluble drugs (such as Ost) in the phospholipid bilayer did not change the charge on the particle surface, so the zeta potential did not change. In addition, the amount of Tf in the Tf-modified Ost liposomes was quantified via BCA assay, and the results showed that the binding efficiency of Tf was $68.56 \pm 8.57\%$.

Figure 2 presents the characterizations of the Tf-modified Ost liposomes. AFM images (Figure 2A and B) reveal that the Tf-modified Ost liposomes were spherical with a smooth surface, with diameters of approximately 100 nm. However, one liposome in the middle of the AFM image is very large, and its particle size may be as high as 300 nm; this could be attributed to the fact that liposomes are relatively flexible and tend to spread out on the mica surface, resulting in an increase in particle size.[40] TEM images (Figure 2C) confirm the spherical morphologies of the Tf-modified Ost liposomes.

The release kinetics of Ost from the free Ost solution, Ost-Lip, and Tf-Ost-Lip were monitored for 72 h in PBS (pH 7.4) containing 10% FBS at 37 °C. It was found that Ost-Lip and Tf-Ost-Lip exhibited controlled release behavior, possibly because most of the Ost molecules were encapsulated in the bilayer membrane and acted as a release barrier to regulate sustained release, which helped to maintain the effective concentration of drugs in the target tissues (Figure 2D).[41] In addition, the storage stability results demonstrate that the particle size, PDI, and encapsulation efficiency of the Ost-Lip and Tf-Ost-Lip changed within a reasonable range after storage for 30 days at room temperature and at 4 °C, indicating that the liposomes had improved stability (Table S1).

Table 1 Particle Size, Zeta Potential, Encapsulation Efficiency, Drug Loading and Tf Binding Efficiency of Liposomes (n=3)

Liposomes	Particle Size (nm)	Polydispersity Index (PDI)	Zeta Potential (mV)	Encapsulation Efficiency (EE) %	Drug Loading (DL) %	Tf Grafting Rate %
Blank liposomes	82.17±3.43	0.163±0.003	−3.11±0.29	—	—	—
Tf-modified blank liposomes	93.46±2.97	0.182±0.004	−6.82±0.52	—	—	63.79±10.08
Osthole liposomes	92.95±4.04	0.179±0.005	−3.48±0.23	93.68±1.81	3.91±0.076	—
Tf-modified osthole liposomes	104.28±3.76	0.194±0.009	−6.95±0.56	92.79±0.96	3.71±0.038	68.56±8.57

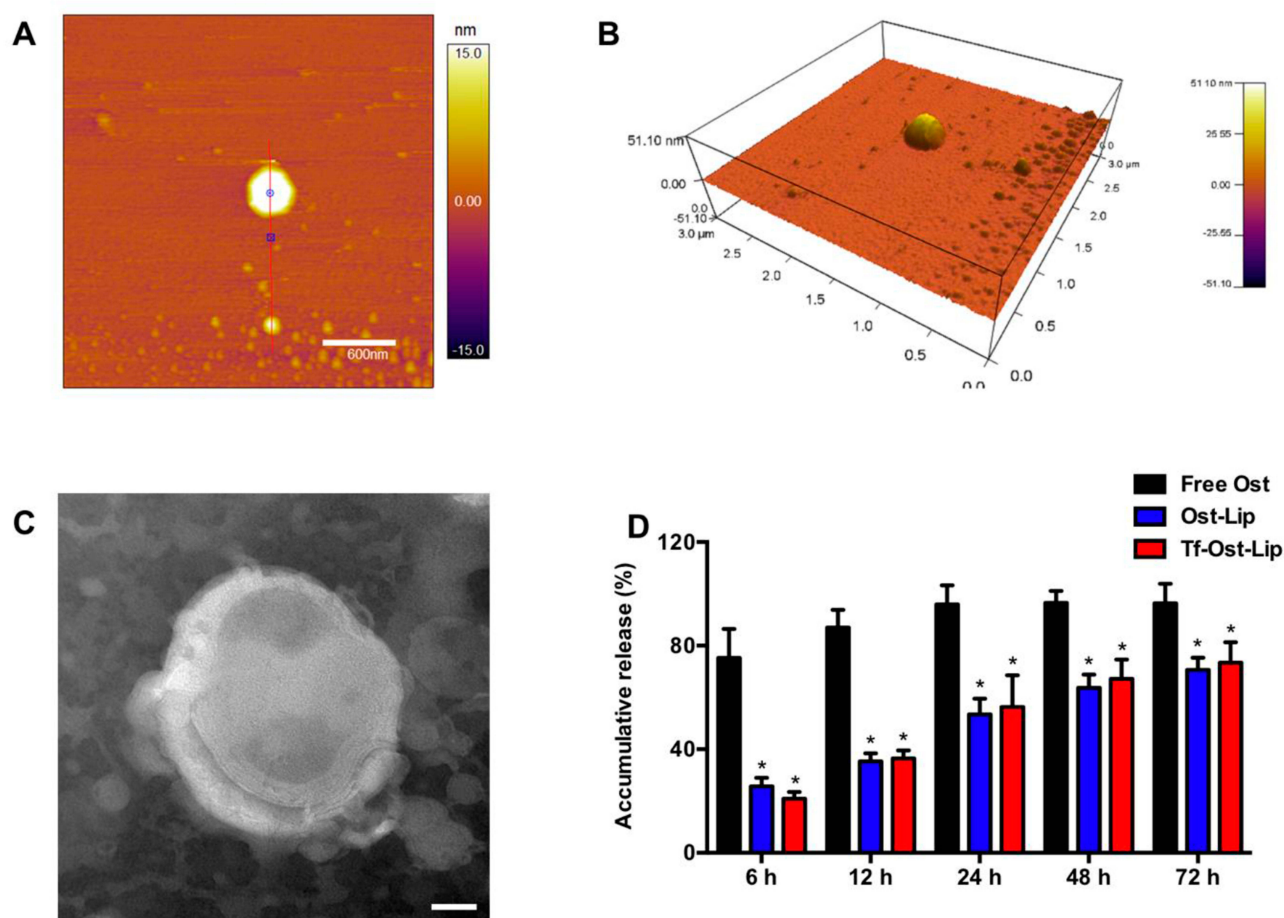**Figure 2** Characterization of Tf-modified osthole liposomes. (**A**) AFM image of Tf-modified osthole liposomes, scalar bar=600 nm. (**B**) 3D structure of (**A**); (**C**) TEM image of Tf-modified osthole liposomes, scalar bar=20 nm; (**D**) Release rate of osthole from the varying formulations. Data are presented as mean ± SD (n=3). * vs Free Ost. $P<0.05$.

Cellular Uptake and Targeting Effects in vitro

According to existing studies on the endocytic mechanism of Ost, it was replaced by RhB dye to determine the intracellular uptake and distribution of the liposome carriers. To assess whether Tf-Ost-Lip could deliver more drugs into cells than other groups of liposomal formulations, hCMEC/D3 cells were chosen as the cell model.[28] Importantly, the fluorescence intensity of Tf-RhB-Lip was found to be 1.61 times greater than that of RhB-Lip, which indicates that Tf-RhB-Lip exhibited better penetrability in hCMEC/D3 cells (Figure 3A and B). Figure 3C and D reveal that the cellular uptake of Tf-RhB-Lip gradually increased with the extension of the incubation time. To obtain direct and visible evidence, the intracellular distributions of the varying formulations were observed via fluorescence microscopy (Figure 3E). The images obtained by the fluorescence microscope were well consistent with the flow cytometry results. Red fluorescence was clearly observed in Tf-RhB-Lip, and was much stronger than that observed in RhB-Lip. All the results indicate that drug accumulation in the Tf-RhB-Lip group was the highest in the hCMEC/D3 cells. Free Tf was added to the culture medium in previous research, and it was found that the free Tf competed with the Tf receptor on the hCMEC/D3 cell membrane and that the uptake of Tf-Lip was significantly reduced, indicating that the transport of liposomes through the BBB is mainly achieved by Tf-mediated endocytosis.[35,42]

Transport Across the BBB Model in vitro

The BBB model in vitro had a low Na-FLU permeability and a TEER value of approximately 250 $\Omega \cdot cm^2$, indicating that the BBB model in vitro requirements were met (results not shown). The intracellular distribution of APP-SH-SY5Y cells in the co-culture BBB model was observed
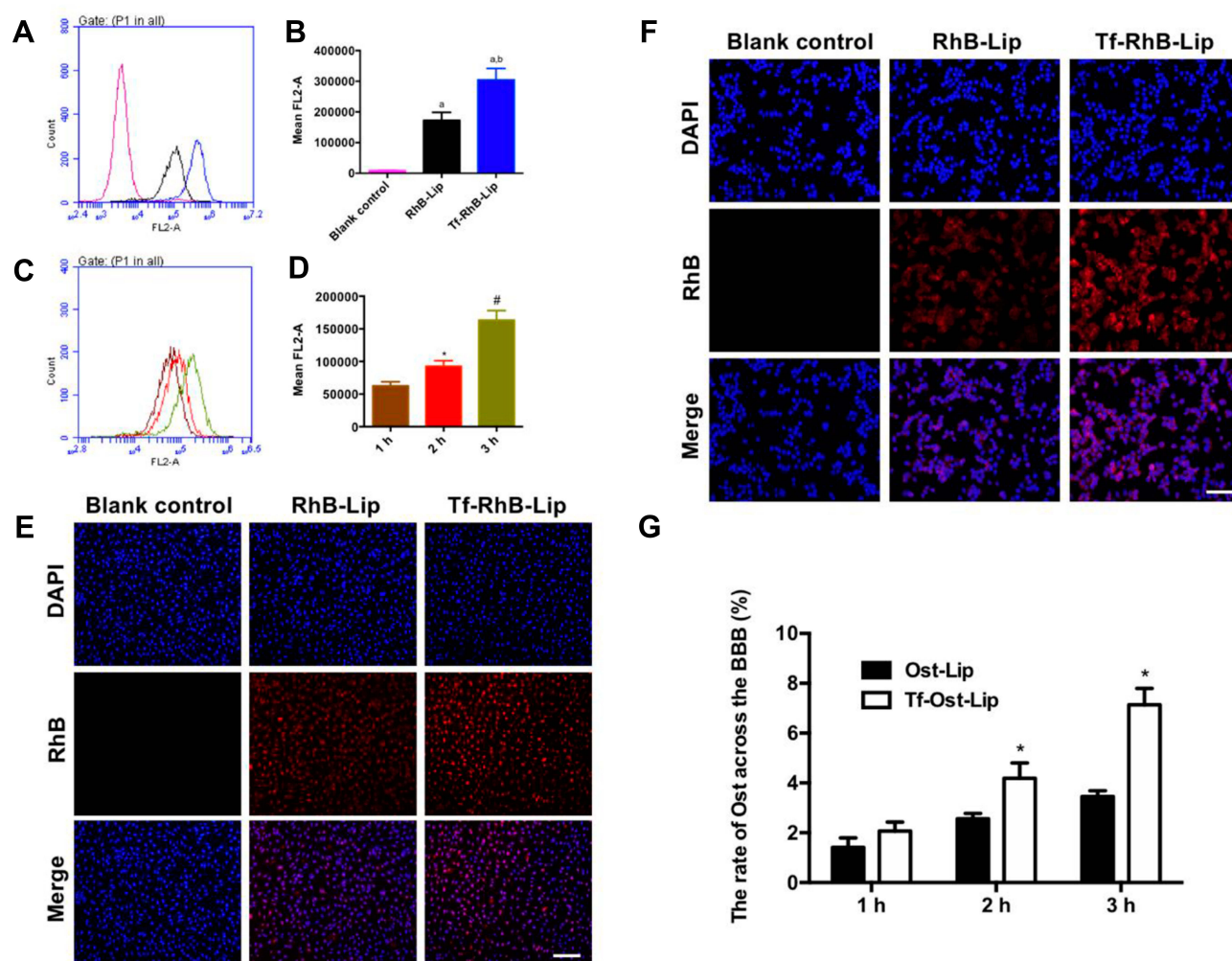
Figure 3 Cellular uptake and distribution after incubation with varying formulations. (**A**) Cellular uptake of hCMEC/D3 cells treated with RhB liposomes and Tf-modified RhB liposomes; (**B**) Quantitative analysis of fluorescence intensity; Data are presented as mean ± SD (n=3). a, vs Blank control; b, vs RhB liposomes. *P*<0.05; (**C**) Cellular uptake of hCMEC/D3 cells treated with Tf-modified RhB liposomes at different time points; (**D**) Quantitative analysis of fluorescence intensity; Data are presented as mean ± SD (n=3). *, vs 1 h; #, vs 2 h. *P*<0.05. (**E**) Analysis of fluorescence intensity of hCMEC/D3 cells incubated with the varying liposomal formulations by fluorescence microscopy, scale bar=100 μm (n=3). (**F**) Cellular uptake of SH-SY5Y incubated with the varying liposomal formulations by fluorescence microscopy in a co-culture model, scale bar=50 μm (n=3). (**G**) The ratio of Ost transported across the BBB in vitro (n=3). *, vs Ost-Lip. *P*<0.05.

via fluorescence microscopy. The results demonstrate that the fluorescence of Tf-RhB-Lip was higher than that of RhB-Lip (Figure 3F). In addition, as shown in Figure 3G, the highest ratio of Ost that could transport across the BBB was found in the Tf-Ost-Lip group, and was significantly higher than that of the Ost-Lip group. Therefore, it is believed that Tf-Ost-Lip has the potential to be used as a carrier to transport drugs across the BBB to treat AD.

The Protective Effect of Tf-Ost-Lip in vitro

To determine the neuroprotective effect of the varying liposomal formulations in vitro, an AD cell model (APP-SH-SY5Y cells) with the overexpression of mutated APP was successfully established.[43] The mutant KM670/671NL gene and the

pCDH-CMV-MCS-EF1-copGFP vector were transfected into SH-SY5Y cells. As shown in Figure 4A, green fluorescence (GFP) was observed in each group of cells under the fluorescence microscope. The expression of the APP protein in the APP group was found to be significantly increased as determined by immunofluorescence and Western blot, but there was almost no APP expression in the GFP group (Figure 4A–C), suggesting that the AD model was successfully established in the SH-SY5Y cells. Next, a CCK-8 assay was used to measure the cell survival of APP-SH-SY5Y cells after treatment with the varying liposomal formulations (100 μM) for 24 h. It was found that Ost-Lip and Tf-Ost-Lip significantly increased the viability from 61.32% to 82.38% and 83.07%, respectively (Figure 4D). The apoptotic rates of APP-SH-SY5Y cells
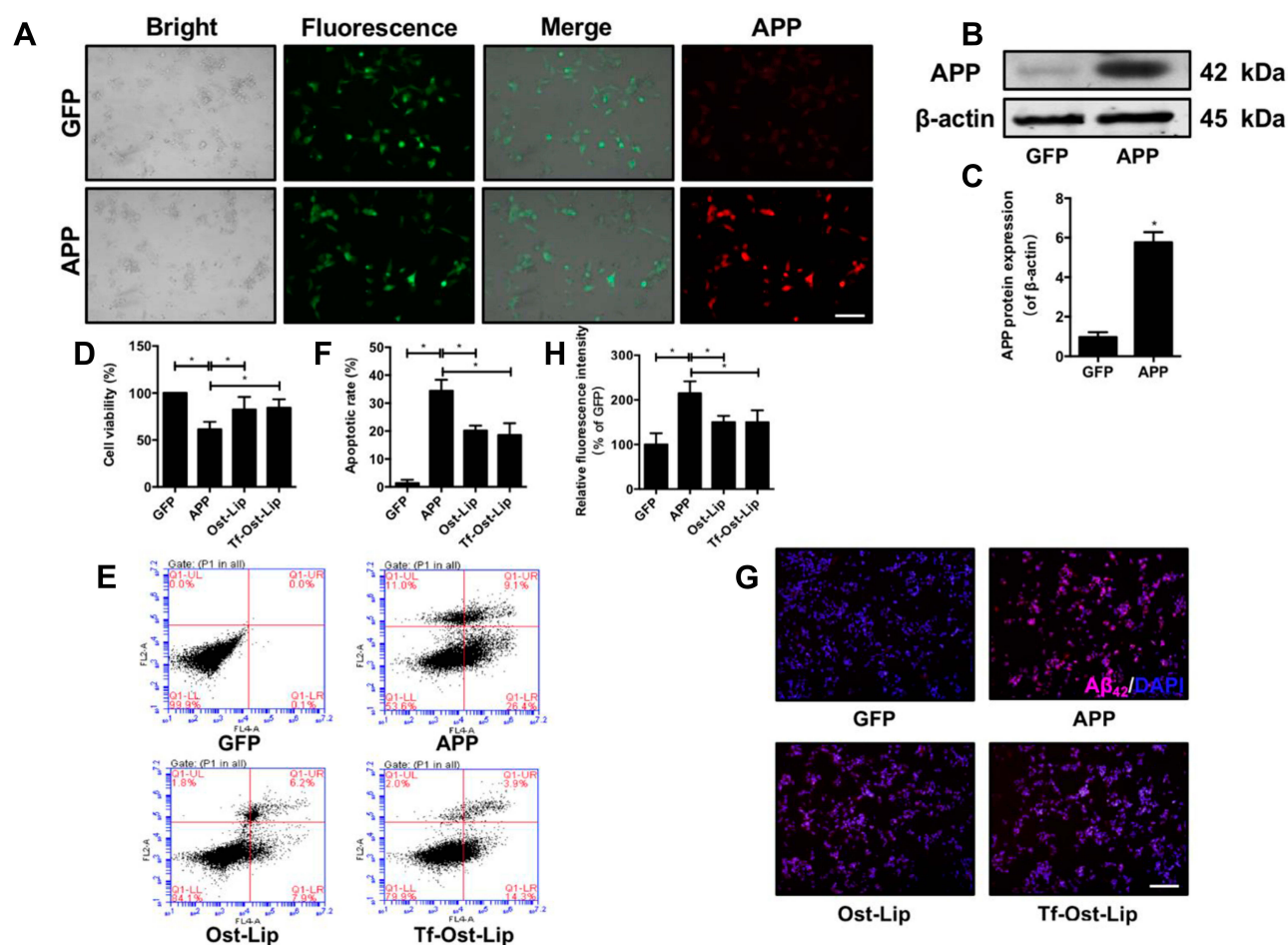
Figure 4 The neuroprotective effect of the varying formulations on APP-SH-SY5Y cells. (**A**) GFP and APP-GFP were transfected into SH-SY5Y cells and APP protein (red) expression was detected by ICC, scale bar=50 μm. (**B**)-(**C**) APP protein expression was detected by Western Blot. (**B**) The representative bands of protein of APP. (**C**) Semi-quantitative analysis of APP protein expression by densitometry. Data are presented as mean±SD (n=3). *$P<0.05$. (**D**) The cell viability was detected by CCK-8 assay. Data are presented as mean±SD (n=6). *$P<0.05$. (**E**) Percentage of apoptotic cells measured by flow cytometry. (**F**) Quantitative analysis of apoptosis in SH-SY5Y cells. Data are presented as mean±SD (n=3). *$P<0.05$. (**G**)-(**H**) $A\beta_{1-42}$ protein expression was detected by immunofluorescent staining. (**G**) Representative images of $A\beta_{1-42}$ in SH-SY5Y cells, scale bar=50 μm (n=6). (**H**) Quantitative analysis of $A\beta 1-42$ proteins expression after treatment with the varying formulations. Data are presented as mean±SD (n=6). *$P<0.05$.

treated with Ost-Lip and Tf-Ost-Lip decreased sequentially. The percentage of apoptotic SH-SY5Y cells in the APP-SH-SY5Y group was 34.43%, and after incubation with Ost-Lip or Tf-Ost-Lip, it decreased to 20.17% and 18.60%, respectively (Figure 4E and F). Furthermore, $A\beta_{42}$ was also detected by immunofluorescence staining. It was found that the APP-SH-SY5Y group showed the strongest fluorescence intensity, and the relative fluorescence intensity of $A\beta_{1-42}$ was reduced after treatment with the varying liposomal formulations (Figure 4G and H). These results indicate that the Ost-loaded liposomes effectively protected neural cells against APP overexpression-induced cytotoxicity. However, the Tf receptor was not expressed on the surface of SH-SY5Y cells, and therefore the protective effect on the overexpression of APP cells was not enhanced by Tf-Ost-Lip.

Pharmacokinetics Analysis

Figure 5A presents the plasma concentration-time curves of Ost after treatment with the varying formulations, and the pharmacokinetic parameters are listed in Table 2. The pharmacokinetic parameters revealed that after the administration of 10 mg/kg of the formulations, the $AUC_{0-48\ h}$ values of the free Ost solution, Ost-Lip, and Tf-Ost-Lip were 0.119 ± 0.027, 2.379 ± 0.577, and 2.448 ± 0.861, respectively. Additionally, the elimination half-life ($t_{1/2\beta}$) was prolonged, the clearance rate (CL) was reduced, and the area under the curve value ($AUC_{0-48\ h}$) was enlarged for Tf-Ost-Lip. These findings indicate that long-circulatory effects in the blood were clearly achieved after the PEGylation on the liposomal surface. The modification of PEG on the liposomes prolonged the
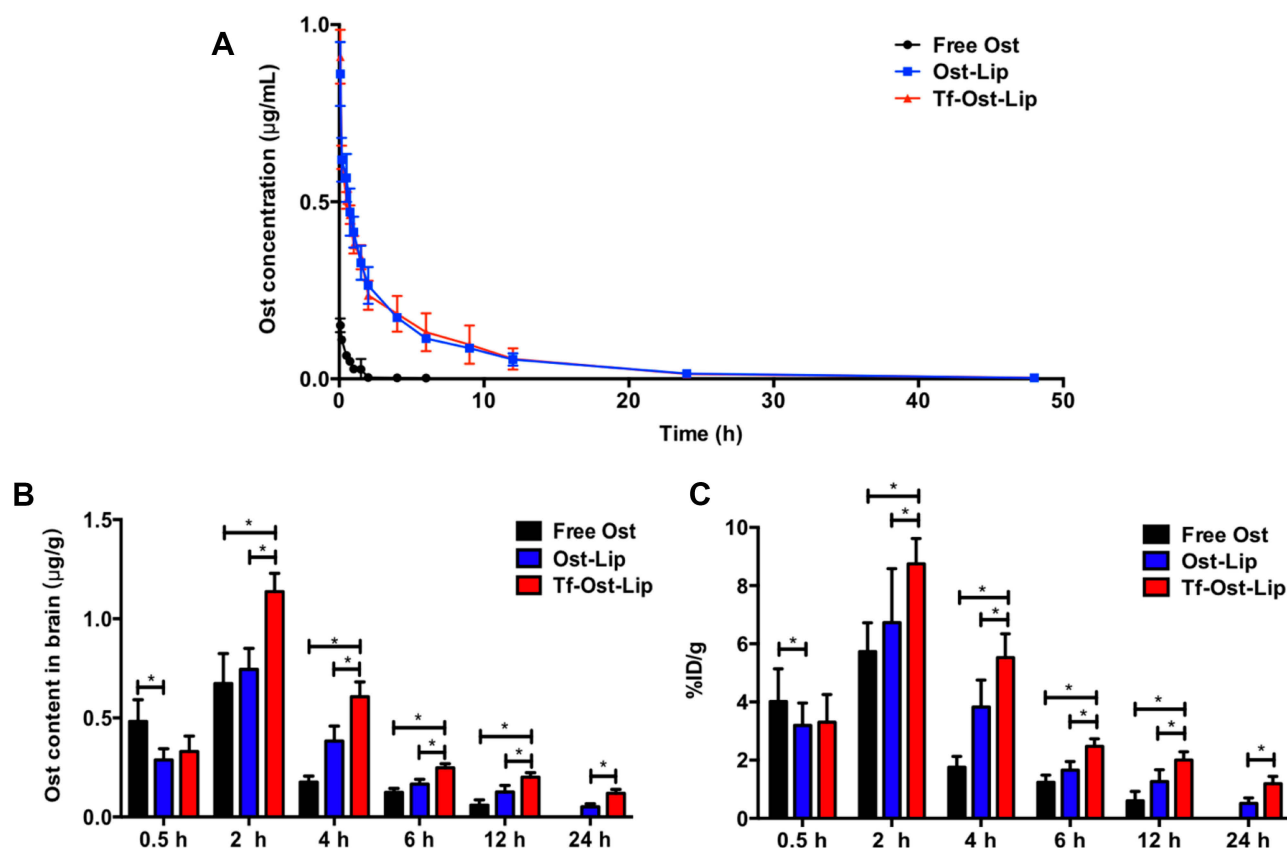
Figure 5 Plasma concentration-time curve of Ost in SD rats and Ost concentration in brain of the varying formulations at different time points. (**A**) Plasma concentration–time curve of Ost pharmacokinetic (PK) profile in SD rats after intravenous administration of the varying formulations (10 mg/kg). (**B**) Drug concentration in brain of APP/PS-1 mice of free Ost solution, Ost-Lip and Tf-Ost-Lip groups at different time points. Data are presented as mean ± SD (n=6). *$P<0.05$. (**C**) %ID/g in brain of APP/PS-1 mice of free Ost solution, Ost-Lip and Tf-Ost-Lip groups at different time points. Data are presented as mean ± SD (n=6). *$P<0.05$.

circulation time via avoiding rapid uptake by the reticuloendothelial system (RES).[44]

Liposome Distribution in the Brain

Due to the integrity of the BBB, drug delivery systems that penetrate the BBB are required to access the brain to have a therapeutic effect on the central nervous system.[6] Several reports have indicated that Tf-modified liposomes could be used to transport drugs through the BBB. To further evaluate the possibility of Tf-Ost-Lip crossing the BBB, the distributions in the brain of Ost in the free Ost solution, Ost-Lip, and Tf-Ost-Lip groups were detected. It was clear that all the formulations could be delivered to the brain through IV administration. The previous results show that the recoveries of Ost plasma and brain tissue samples were good, and the standard curves were linear (data not shown). The quantitative results are presented in Figure 5B and C, and it was found that the drug content in the brain after Tf modification was higher than that in the unmodified liposomes group, and much higher than that in the free Ost solution group, at all the predetermined time points. The drug content in the free Ost solution group decreased rapidly over 24 h, which may have been caused by drug outflow and metabolism. However, the drug content in the brain of the liposomes groups decreased slowly because of the sustained release effect of the liposomes. The pharmacokinetic parameters of the brain are presented in Table 3. The

Table 2 Pharmacokinetic Parameters of Ost Following Intravenous Administration of the Varying Formulations in SD Rats at 10 Mg/Kg Ost Dose (n = 6)

Parameters	Free Ost	Ost-Lip	Tf-Ost-Lip
$t_{1/2\alpha}$ (h)	0.172±0.237	0.216±0.314	0.200±0.250
$t_{1/2\beta}$ (h)	0.602±0.303	3.673±2.281	3.382±1.239
V_1 (L/kg)	67.501±16.848	13.702±6.556	14.891±9.106
CL (L/h/g)	154.769±30.508	8.461±1.937	8.326±2.348
AUC$_{0-48\ h}$ (mg/L/h)	0.119±0.027	2.379±0.577	2.488±0.861

Table 3 Pharmacokinetic Parameters of Ost in Brain After Administration of Varying Formulations (n = 6)

Formulation	$AUC_{0-24\ h}$ (µg/g/h)	C_{max} (µg/g)	t_{max} (h)	MRT (h)	Re	Ce
Free Ost	344.82±67.16	0.71±0.17	2	6.39±0.51	—	—
Ost-Lip	489.19±60.31	0.75±0.11	2	7.85±0.08	1.39	1.25
Tf-Ost-Lip	791.63±72.89	1.46±0.38	2	7.33±0.38	3.74	3.38

results reveal that the AUC_{0-24h} and C_{max} values of Ost from Tf-modified liposomes were fairly greater than those of free Ost. The relative uptake efficiencies (Re) of Ost-Lip and Tf-Ost-Lip were enhanced to 1.39 and 3.74 times than that of free Ost, respectively. The concentration efficiencies (Ce) were also respectively enhanced to 1.25 and 3.38 times than that of free Ost. This data further proves that Ost-Lip modified with Tf presented superior brain-targeting efficiency.[45]

Imaging of Liposomes in APP/PS-1 Mice

To observe the brain-targeting ability of the liposomes, Ost was replaced with DiR dye. The results reveal that the administration of different formulations, including the free Ost solution, Ost-Lip, and Tf-Ost-Lip, resulted in different brain-targeting effects. Figure 6 presents the representative images of APP/PS-1 mice after administration with varying formulations. The results indicate that free DiR was primarily distributed in the liver throughout the whole experiment, and little fluorescent signal was detected in the brain. In contrast, strong fluorescent signals were observed in the brain after the administration of DiR liposomes and Tf-modified DiR liposomes, and the signals in the Tf-modified DiR liposome group were maintained for up to 24 h. The reason that the whole-body fluorescence was too strong at 0–3 h may have been due to the addition of long-circulation materials to the liposomes, which prolonged the circulation time of DiR in the blood and resulted in enhanced fluorescence signals. Another possible reason is because APP/PS-1 transgenic mice, which are of the C57BL/6 strain, were used, and the strong fluorescence signal can also be associated with hair interference in mice. However, it is evident from the comparison between groups that the fluorescence signal of the brain tissue after Tf modification was notably enhanced, which can explain its brain-targeting ability to a certain extent.

The Protective Effect of Tf-Ost-Lip in vivo

It is well known that the key factor for neuronal injury and loss is neuronal apoptosis. It plays a crucial role in many central nervous system degenerative diseases, including AD, and its processes mainly affect the Bcl-2 family and caspases.[46] The Bcl-2 family consists of pro-apoptotic proteins (Bax, Bad, and BAK) and anti-apoptotic proteins (Bcl-2 and Bcl-XL). BAD can increase mitochondrial permeability, release pro-apoptotic factors and CytC, and bind to Bcl-2 family proteins to form dimers, which trigger caspase signaling and cleave pro-caspase-3 into its active forms, resulting in neuronal apoptosis.[47] There is increasing evidence that oxidative stress and neuroinflammation play an important role in the mechanisms associated with Aβ-induced neurotoxicity in AD.[48] Aggregated Aβ may induce oxidative stress by causing mitochondrial dysfunction, which induces the release of reactive oxygen species (ROS), reduces antioxidant levels, such as those of superoxide dismutase (SOD), glutathione peroxidase (GSH-Px), etc., and increases oxidant levels, such as those of malondialdehyde (MDA).[49] Aβ aggregates may induce oxidative stress; in turn, oxidative stress accelerates the production and accumulation of Aβ, thereby promoting the progression of AD. Moreover, Aβ triggers the activation of microglia, which induces the production of pro-inflammatory factors, particularly tumor necrosis factor alpha (TNF-α), interleukin-1β (IL-1β), and interleukin-6 (IL-6). This induces chronic neuroinflammation, may promote synaptic loss and cognitive dysfunction, and ultimately leads to neuronal apoptosis and loss.[50,51] Therefore, the suppression of Aβ-induced neurotoxicity and inhibition of apoptosis, oxidative stress, and neuroinflammation are attractive strategies for the treatment of AD.

Figures 7 and 8 present the neuroprotective effects of the varying formulations on APP/PS-1 mice. According to Figure 7A, all the drug treated groups showed different degrees of apoptosis inhibition as compared to the control group. The Bax-positive and cleaved caspase-3-positive cells were significantly decreased in the regions of the hippocampus and cerebral cortex of the mice in the treatment groups as compared with those of the mice in the APP/PS-1group. Additionally, Bcl-2-positive cells were significantly increased in the groups with varying formulations. Among them, Tf-Ost-Lip had the strongest regulatory effects on Bax, Bcl-2, and cleaved caspase-3.
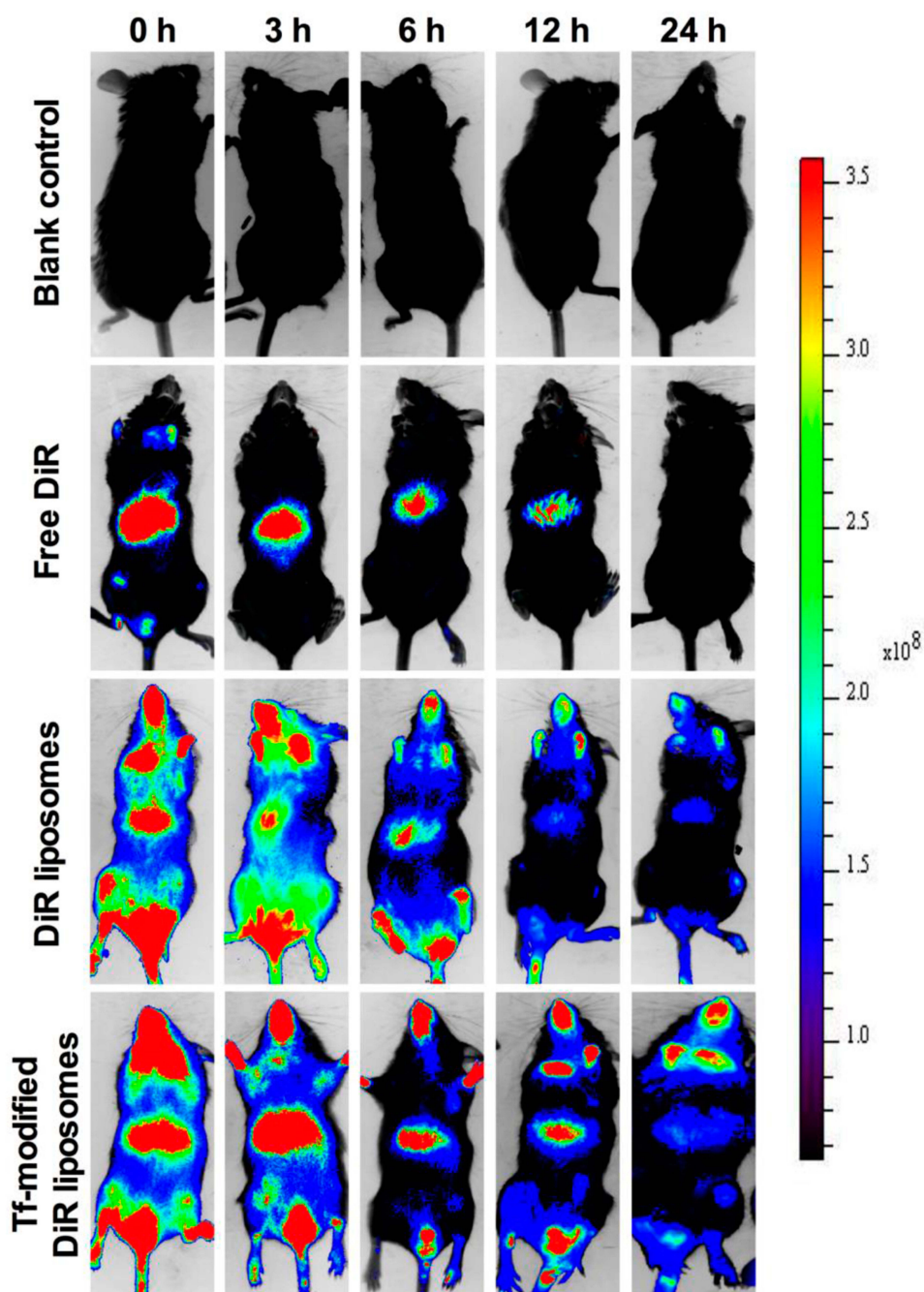
Figure 6 Real-time imaging observation after intravenous administration of varying liposomal formulations in APP/PS-1 mice (n=3).

Regarding oxidative stress, the MDA content decreased and SOD activity increased in the brains of Tf-Ost-Lip-treated APP/PS-1 mice with respect to the untreated mice (Figure 7B and C). Concerning neuroinflammation, the TNF-α, IL-6, and IL-1β levels and Iba-1 expression of treated APP/PS-1 mice were lower than those of the untreated mice at the end of treatment, whereas decreased in the treatment groups with the greatest decreased in the Tf-Ost-Lip treatment (Figure 7D–G).

In the subsequent experiments, Aβ plaque deposits in the cortex and hippocampus of the brain were observed after treatment with the varying formulations. The results indicate that amyloid deposition was intense in the brains of the APP/PS-1 mice, while it was significantly reduced in the brains of the APP/PS-1 mice after Tf-Ost-Lip treatment (Figure 7H). Moreover, $Aβ_{1–42}$ protein expression was detected by Western blot analysis, and it was found that the expressions of the $Aβ_{1–42}$ protein were decreased after
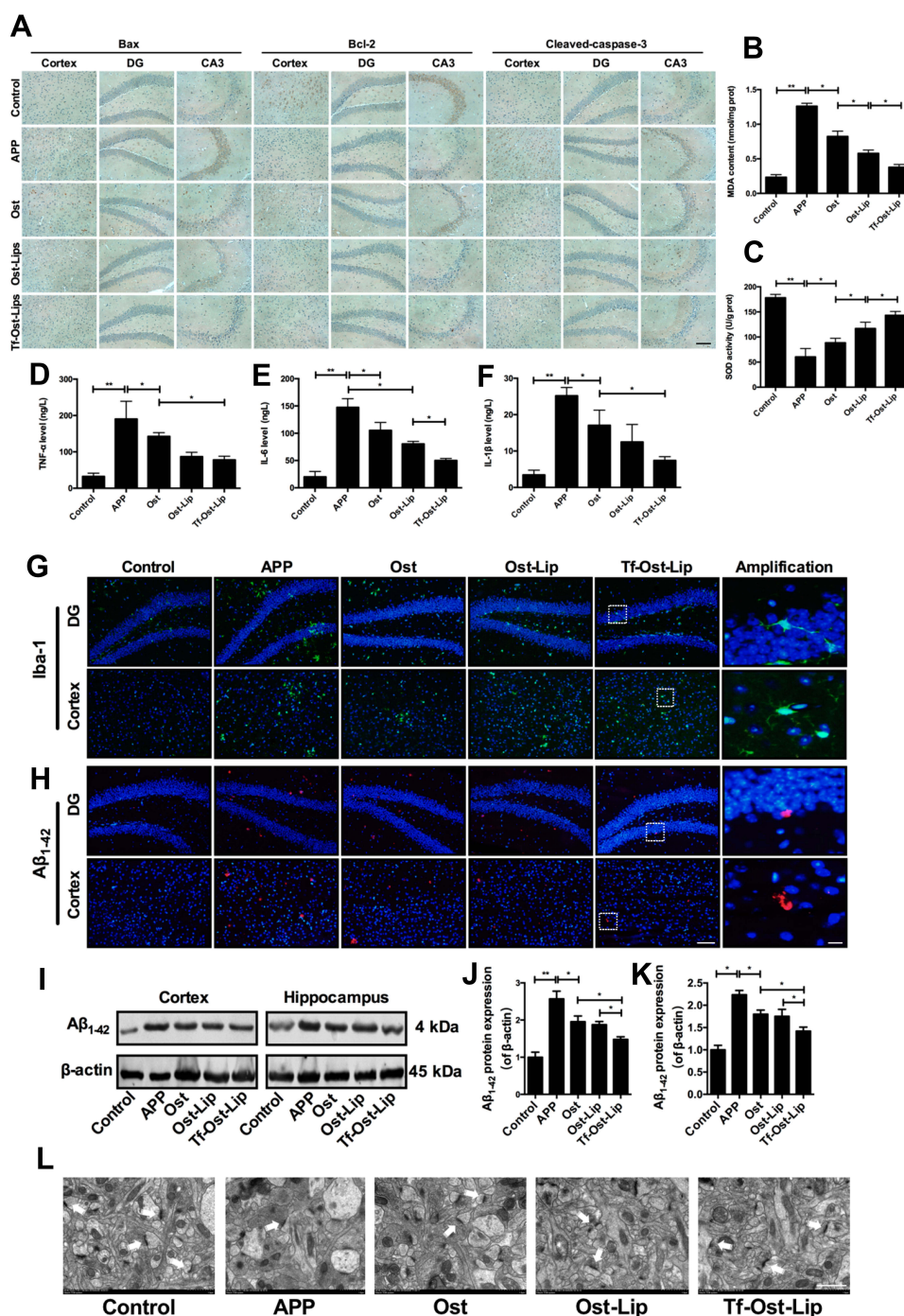
Figure 7 The neuroprotective effect of the varying formulations on APP/PS-1 mice. (**A**) The expression of Bax, Bcl-2 and Cleaved-caspase-3 detected by immunohistochemistry staining in hippocampus and cortex of APP/PS-1 mice, scale bar=50 μm (n=6). (**B**)-(**C**) Effect of the varying formulations on brain oxidative stress. The content of MDA (**B**) and the activity of SOD (**C**) in brain tissues detected by Kits. Data are presented as mean±SD (n=6). *$P<0.05$, **$P<0.01$. (**D**)-(**F**) Effect of the varying formulations on neuroinflammation. The levels of TNF-α (**D**), IL-6 (**E**) and IL-1β (**F**) in brain tissues detected by ELISA. Data are presented as mean±SD (n=6). *$P<0.05$, **$P<0.01$. (**G**) Representative images of microglia (Iba-1) in hippocampus and cortex of APP/PS-1 mice by Immunofluorescence staining, scale bar=50 μm, scale bar=10 μm in the insets (n=6). (**H**) Representative images of Aβ$_{1-42}$ plaques in hippocampus and cortex by Immunofluorescence staining, scale bar=50 μm, scale bar=10 μm in the insets (n=6). (**I**) The representative bands of proteins of Aβ$_{1-42}$. (**J**)-(**K**) Semi-quantitative analysis of Aβ$_{1-42}$ proteins expression by densitometry in the cortex (**J**) and hippocampus (**K**) after treatment with the varying formulations. Data are presented as mean±SD (n=6). *$P<0.05$, **$P<0.01$. (**L**) Electron microscopic images from hippocampal CA1 stratum radiatum regions of Control, APP, Ost, Ost-Lip and Tf-Ost-Lip groups. White arrows indicate normal synapses, scale bar=1 μm (n=6).

treatment with the varying formulations. The Aβ$_{1-42}$ protein was found to be significantly down-regulated for Tf-Ost-Lip (Figure 7I–K). Furthermore, the ultrastructures of

hippocampal neurons in the mice with and without treatment were compared. As presented in Figure 7L, in the control mice, neurons in the hippocampus appeared normal
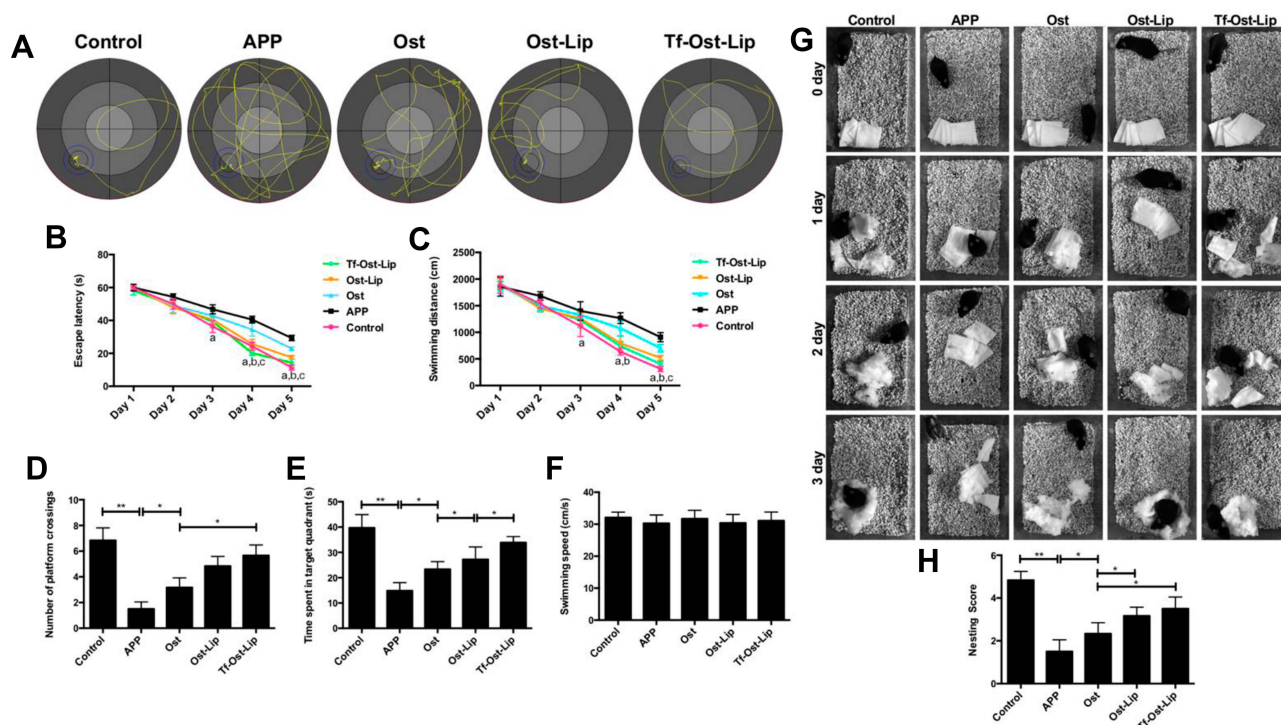
Figure 8 The therapeutic effects of the varying formulations on the cognitive decline of APP/PS-1 mice. (**A**)-(**F**) The learning ability of different groups of mice was determined by MWM. (**A**) The representative swimming paths in the water maze trial on day 5. (**B**) Escape latency of the water maze task. (**C**) Swimming distance in the formal experimentals of the water maze task. Data are presented as mean ± SD (n=6). a, vs APP; b, vs Ost; c, vs Ost-Lip. $P<0.05$. (**D**) Times of crossing the removed-platform. (**E**) The time spent of mice in the target quadrant. (**F**) Swimming speed of mice. Data are presented as mean ± SD (n=6). *$P<0.05$, **$P<0.01$. (**G**–**H**) Effects of the varying formulations on nest building behavior in APP/PS-1 mice. (**G**) Representative images were obtained from 0 to 3 days. (**H**) Analysis of nesting score in APP/PS-1 mice after treatment with the varying formulations. Data are presented as mean ± SD (n=6). *$P<0.05$, **$P<0.01$.

in morphology, and the organelles were well arranged. However, in the APP/PS-1 mice, hippocampal neurons were obviously impaired and synapses were reduced, and postsynaptic membrane thickening and loss of the synaptic cleft were observed. More normal mitochondria were found in the Ost-Lip and Tf-Ost-Lip mice groups, the synaptic cleft was clear without obvious widening, and the postsynaptic density was centralized.

The MWM was employed to investigate the effects of the varying formulations on the spatial memory and learning ability of APP/PS-1 mice.[29,52,53] During the navigation test, the untreated APP/PS-1 mice showed definite learning deficits, whereas the treated APP/PS-1 mice clearly exhibited improved learning ability (Figure 8A–C). The platform was removed in the probe trial to measure the memory function on the 6th day of the test. It was found that the untreated APP/PS-1 mice showed no preference toward the target quadrant, so apparent memory impairment was observed; in contrast, the Tf-Ost-Lip-treated APP/PS-1 mice performed better than those in the Ost-Lip group (Figure 8D–F). In addition, these observations

were further confirmed by nest-building experiments, in which similar results were obtained (Figure 8G–H). More importantly, according to these results, it can be explained to some extent that Tf-Ost-Lip has a better ability to improve cognitive function in APP/PS-1 mice than does free Ost and Ost-Lip.

Conclusion

In this study, Tf-modified Ost liposomes were prepared and evaluated as a treatment for AD, as they contribute targeting ability to enhance the permeability of Ost across the BBB. In addition, Tf-Ost-Lip protects APP-SH-SY5Y cells against neurotoxicity, attenuates Aβ plaque deposition, and inhibits apoptosis, oxidative stress, and neuroinflammation in APP/PS-1 mice. In conclusion, it was demonstrated that Tf-Ost-Lip could enhance anti-AD effects both in vitro and in vivo, which can be attributed to the following. (i) The addition of a hydrophilic material prevents the rapid absorption of the reticuloendothelial system, thereby prolonging the blood circulation time of drugs. (ii) The modification of Tf on the surfaces of liposomes can promote the penetration

of drugs into the BBB via an endocytosis mechanism, and can increase the accumulation of drugs in the lesion areas. It is believed that Tf-Ost-Lip may be a promising strategy for the treatment of Alzheimer's disease. Although pharmacodynamic and pharmacokinetic studies in vivo have confirmed that Tf-Ost-Lip has long-term circulation, controlled release, and targeting effects, the research objects of laboratory animal models cannot fully represent practical clinical applications. Currently, targeted long-circulation liposomes are mainly in the laboratory exploration stage, and there exist few drugs in clinical trials. Their industrialization has several key issues, such as stability, sterilization methods, encapsulation efficiency, and cytotoxicity, among others.[54,55] Therefore, dialogue between scientists, clinicians, and the industry is essential for the production of circulated liposomes with higher safety, better quality and stability, and lower production costs.

Abbreviations

AD, Alzheimer's disease; Aβ, β-amyloid polypeptide; BBB, Blood-brain barrier; Lip, Liposomes; Tf, Transferrin; Ost, Osthole; BACE1, Beta secretase 1; EPC, Egg yolk phosphatidylcholine; Chol, Cholesterol; HEPES, 2-[4-(2-hydroxyethyl)piperazin-1-yl]ethanesulfonic acid; DAPI, 4′,6-diamidino-2-phenylindole; DiR, 1.1-dioctadecyl-3,3,3,3- tetramethylindotricarbocyanine iodide; CCK-8, The cell counting kit-8; SH-SY5Y, Human neuroblastoma cells; HEK293T, Human embryonic kidney cells; hCMEC/D3, Human brain endothelial cells; PBS, Phosphate buffer saline; RES, Reticuloendothelial system; HPLC, High performance liquid chromatography; ROS, Reactive oxygen species; SOD, Superoxide dismutase; MDA, Malondialdehyde; TNF-α, Tumor necrosis factor alpha; IL-1β, Interleukin-1β; IL-6, Interleukin-6; HRP, Horseradish Peroxidase; APP, Amyloid precursor protein; SD rats, Sprague-Dawley rats; FLU, Fluorescein disodium salt; TEER, transendothelial electrical resistance.

Acknowledgments

Disclosure

The authors report no conflicts of interest in this work.

References

1. Chang KW, Zong HF, Ma KG, et al. Activation of alpha7 nicotinic acetylcholine receptor alleviates Abeta1-42-induced neurotoxicity via downregulation of p38 and JNK MAPK signaling pathways. *Neurochem Int*. 2018;120:238–250. doi:10.1016/j.neuint.2018.09.005

2. Li F, Zhang Y, Lu X, Shi J, Gong Q. Icariin improves the cognitive function of APP/PS-1 mice via suppressing endoplasmic reticulum stress. *Life Sci*. 2019;234:116739. doi:10.1016/j.lfs.2019.116739

3. Li X, Lu J, Xu Y, et al. Discovery of nitazoxanide-based derivatives as autophagy activators for the treatment of Alzheimer's disease. *Acta Pharm Sin B*. 2019.

4. Panza F, Lozupone M, Seripa D, Imbimbo BP. Amyloid-beta immunotherapy for alzheimer disease: is it now a long shot? *Ann Neurol*. 2019;85(3):303–315. doi:10.1002/ana.25410

5. Bouter Y, Lopez Noguerola JS, Tucholla P, et al. Abeta targets of the biosimilar antibodies of bapineuzumab, crenezumab, solanezumab in comparison to an antibody against N-truncated abeta in sporadic Alzheimer disease cases and mouse models. *Acta Neuropathol*. 2015;130(5):713–729. doi:10.1007/s00401-015-1489-x

6. Agrawal M, Saraf S, Tripathi DK, et al. Recent advancements in liposomes targeting strategies to cross blood-brain barrier (BBB) for the treatment of Alzheimer's disease. *J Control Release*. 2017; 260:61–77. doi:10.1016/j.jconrel.2017.05.019

7. Wong KH, Riaz MK, Xie Y, et al. Review of current strategies for delivering alzheimer's disease drugs across the blood-brain barrier. *Int J Mol Sci*. 2019;20(2):381. doi:10.3390/ijms20020381

8. Magro RD, Cox A, Zembelli V, et al. The ability of liposomes, tailored for blood-brain barrier targeting, to reach the brain is dramatically affected by the disease state. *Nanomedicine*. 2018;13 (6):585–594. doi:10.2217/nnm-2017-0317

9. Agrawal M, Saraf S, Saraf S, et al. Recent advancements in the field of nanotechnology for the delivery of anti-Alzheimer drug in the brain region. *Expert Opin Drug Deliv*. 2018;15(6):589–617. doi:10.1080/17425247.2018.1471058

10. Singh M, Thakur V, Deshmukh R, et al. Development and characterization of morin hydrate-loaded micellar nanocarriers for the effective management of Alzheimer's disease. *J Microencapsul*. 2018;35 (2):137–148. doi:10.1080/02652048.2018.1441916

11. Alexander A, Agrawal M, Uddin A, et al. Recent expansions of novel strategies towards the drug targeting into the brain. *Int J Nanomedicine*. 2019;14:5895–5909. doi:10.2147/IJN.S210876

12. Ross C, Taylor M, Fullwood N, Allsop D. Liposome delivery systems for the treatment of Alzheimer's disease. *Int J Nanomedicine*. 2018;13:8507–8522. doi:10.2147/IJN.S183117

13. Ordonez-Gutierrez L, Posado-Fernandez A, Ahmadvand D, et al. ImmunoPEGliposome-mediated reduction of blood and brain amyloid levels in a mouse model of Alzheimer's disease is restricted to aged animals. *Biomater*. 2017;112:141–152. doi:10.1016/j.biomaterials.2016.07.027

14. Corace G, Angeloni C, Malaguti M, et al. Multifunctional liposomes for nasal delivery of the anti-Alzheimer drug tacrine hydrochloride. *J Liposome Res*. 2014;24(4):323–335. doi:10.3109/08982104.2014.899369

15. Gao JQ, Lv Q, Li LM, et al. Glioma targeting and blood-brain barrier penetration by dual-targeting doxorubincin liposomes. *Biomater*. 2013;34(22):5628–5639. doi:10.1016/j.biomaterials.2013.03.097

16. Gothwal A, Nakhate KT, Ajazuddin AA, Gupta U. boosted memory and improved brain bioavailability of rivastigmine: targeting effort to the brain using covalently tethered lower generation PAMAM dendrimers with lactoferrin. *Mol Pharm*. 2018;15(10):4538–4549. doi:10.1021/acs.molpharmaceut.8b00537

17. Papadia K, Giannou AD, Markoutsa E, et al. Multifunctional LUV liposomes decorated for BBB and amyloid targeting - B. in vivo brain targeting potential in wild-type and APP/PS-1 mice. *eur J Pharm Sci*. 2017;102:180–187. doi:10.1016/j.ejps.2017.03.010

18. Kuo YC, Chou PR. Neuroprotection against degeneration of SK-N-MC cells using neuron growth factor-encapsulated liposomes with surface cereport and transferrin. *J Pharm Sci*. 2014;103 (8):2484–2497. doi:10.1002/jps.24081

19. Yan YH, Li SH, Li HY, Lin Y, Yang JX. Osthole protects bone marrow-derived neural stem cells from oxidative damage through PI3K/Akt-1 pathway. *Neurochem Res*. 2017;42(2):398–405. doi:10. 1007/s11064-016-2082-y

20. Xia Y, Kong L, Yao Y, et al. Osthole confers neuroprotection against cortical stab wound injury and attenuates secondary brain injury. *J Neuroinflammation*. 2015;12(1):155. doi:10.1186/s12974-015-0373-x

21. Li SH, Gao P, Wang LT, et al. Osthole stimulated neural stem cells differentiation into neurons in an alzheimer's disease cell model via upregulation of microRNA-9 and rescued the functional Impairment of hippocampal neurons in APP/PS-1 transgenic mice. *Front Neurosci*. 2017;11:340. doi:10.3389/fnins.20 17.00340

22. Jiao Y, Kong L, Yao Y, et al. Osthole decreases beta amyloid levels through up-regulation of miR-107 in Alzheimer's disease. *Neuropharmacol*. 2016;108:332–344. doi:10.1016/j.neuropharm.20 16.04.046

23. Chu Q, Zhu Y, Cao T, et al. Studies on the neuroprotection of osthole on glutamate-induced apoptotic cells and an alzheimer's disease mouse model via modulation oxidative stress. *Appl Biochem Biotechnol*. 2019;190(2):634–644.

24. Yang YF, Xu W, Song W, Ye M, Yang XW. Transport of twelve coumarins from angelicae pubescentis radix across a MDCK-pHaMDR cell monolayer-an in vitro model for blood-brain barrier permeability. *Molecules*. 2015;20(7):11719–11732. doi:10.339 0/molecules200711719

25. Wang Y, Yang Y, Yu Y, et al. Transferrin modified dioscin loaded PEGylated liposomes: characterization and in vitro antitumor effect. *J Nanosci Nanotechnol*. 2019;20(3):1321–1331. doi:10.1166/jnn.20 20.16955

26. Li XY, Zhao Y, Sun MG, et al. Multifunctional liposomes loaded with paclitaxel and artemether for treatment of invasive brain glioma. *Biomater*. 2014;35(21):5591–5604. doi:10.1016/j.biomaterials.2014. 03.049

27. Re F, Cambianica I, Sesana S, et al. Functionalization with ApoE-derived peptides enhances the interaction with brain capillary endothelial cells of nanoliposomes binding amyloid-beta peptide. *J Biotechnol*. 2011;156(4):341–346. doi:10.1016/j.jbiotec.2011.06. 037

28. Yin T, Xie W, Sun J, Yang L, Liu J. Penetratin peptide-functionalized gold nanostars: enhanced BBB permeability and NIR photothermal treatment of Alzheimer's disease using ultralow irradiance. *ACS Appl Mater Interfaces*. 2016;8(30):19291–19302. doi:10.1021/acsami.6b0 5089

29. Meng T, Cao Q, Lei P, et al. Tat-haFGF14-154 upregulates ADAM10 to attenuate the Alzheimer phenotype of APP/PS-1 mice through the PI3K-CREB-IRE1alpha/XBP1 pathway. *Mol Ther Nucleic Acids*. 2017;7:439–452. doi:10.1016/j.omtn.2017.05.004

30. Zhang Z, Yang J, Liu C, et al. Pseudoginsenoside-F11 alleviates cognitive deficits and Alzheimer's disease-type pathologies in SAMP8 mice. *Pharmacol Res*. 2019;139:512–523. doi:10.1016/j. phrs.2018.10.024

31. Yeh CW, Yeh SH, Shie FS, et al. Impaired cognition and cerebral glucose regulation are associated with astrocyte activation in the parenchyma of metabolically stressed APPswe/PS1dE9 mice. *Neurobiol Aging*. 2015;36(11):2984–2994. doi:10.1016/j.neurobiolaging.2015. 07.022

32. Sun J, Wei C, Liu Y, et al. Progressive release of mesoporous nano-selenium delivery system for the multi-channel synergistic treatment of Alzheimer's disease. *Biomater*. 2019;197:417–431. doi:10.1016/j. biomaterials.2018.12.027

33. Alexander A, Saraf S. Nose-to-brain drug delivery approach: a key to easily accessing the brain for the treatment of Alzheimer's disease. *Neural Regen Res*. 2018;13(12):2102–2104. doi:10.4103/1673-5374.241458

34. Agrawal M, Saraf S, Saraf S, et al. Nose-to-brain drug delivery: an update on clinical challenges and progress towards approval of anti-Alzheimer drugs. *J Control Release*. 2018;281:139–177. doi:10. 1016/j.jconrel.2018.05.011

35. Chen ZL, Huang M, Wang XR, et al. Transferrin-modified liposome promotes alpha-mangostin to penetrate the blood-brain barrier. *Nanomed Nanotechnol Biol Med*. 2016;12(2):421–430. doi:10.1016/ j.nano.2015.10.021

36. Sonali S, Singh RP, Singh N, et al. Transferrin liposomes of docetaxel for brain targeted cancer applications: formulation and brain theranostics. *Drug Deliv*. 2016;23(4):1261–1271. doi:10.3109/ 10717544.2016.1162878

37. Lakkadwala S, Dos Santos Rodrigues B, Sun C, Singh J. Dual functionalized liposomes for efficient co-delivery of anti-cancer chemotherapeutics for the treatment of glioblastoma. *J Control Release*. 2019;307:247–260. doi:10.1016/j.jconrel.2019.06.033

38. Xiao W, Xiong J, Zhang S, et al. Influence of ligands property and particle size of gold nanoparticles on the protein adsorption and corresponding targeting ability. *Int J Pharm*. 2018;538(1–2):105–111. doi:10.1016/j.ijpharm.2018.01.011

39. Emami J, Rezazadeh M, Sadeghi H, et al. Development and optimization of transferrin-conjugated nanostructured lipid carriers for brain delivery of paclitaxel using box–behnken design. *Pharm Dev Technol*. 2016;22(3):370–382. doi:10.1080/10837450.2016.1189933

40. Anabousi S, Laue M, Lehr CM, et al. Assessing transferrin modification of liposomes by atomic force microscopy and transmission electron microscopy. *Eur J Pharm Biopharm*. 2005;60(2):295–303. doi:10.1016/j.ejpb.2004.12.009

41. Binda A, Panariti A, Barbuti A, et al. Modulation of the intrinsic neuronal excitability by multifunctional liposomes tailored for the treatment of Alzheimer's disease. *Int J Nanomedicine*. 2018;13:4059–4071. doi:10.2147/IJN.S161563

42. Ju RJ, Li XT, Shi JF, et al. Liposomes, modified with PTD(HIV-1) peptide, containing epirubicin and celecoxib, to target vasculogenic mimicry channels in invasive breast cancer. *Biomater*. 2014;35 (26):7610–7621. doi:10.1016/j.biomaterials.2014.05.040

43. Dubey SK, Ram MS, Krishna KV, et al. Recent expansions on cellular models to uncover the scientific barriers towards drug development for Alzheimer's disease. *Cell Mol Neurobiol*. 2019;39 (2):181–209. doi:10.1007/s10571-019-00653-z

44. Xiao Y, Liu Q, Clulow AJ, et al. PEGylation and surface functionalization of liposomes containing drug nanocrystals for cell-targeted delivery. *Colloids Surf B*. 2019;182:110362. doi:10.1016/j. colsurfb.2019.110362

45. Guo JW, Guan PP, Ding WY, et al. Erythrocyte membrane-encapsulated celecoxib improves the cognitive decline of Alzheimer's disease by concurrently inducing neurogenesis and reducing apoptosis in APP/PS-1 transgenic mice. *Biomater*. 2017;145:106–127. doi:10.1016/j.biomaterials.2017.07.023

46. He J, Ji X, Li Y, et al. Subchronic exposure of benzo(a)pyrene interferes with the expression of Bcl-2, Ki-67, C-myc and p53, Bax, Caspase-3 in sub-regions of cerebral cortex and hippocampus. *Exp Toxicol Pathol*. 2016;68(2–3):149–156. doi:10.1016/j.etp.2015.11.007

47. Wang X, Wu J, Yu C, et al. Lychee seed saponins improve cognitive function and prevent neuronal injury via inhibiting neuronal apoptosis in a rat model of Alzheimer's disease. *Nutrients*. 2017;9(2):105. doi:10.3390/nu9020105

48. Guerriero F, Sgarlata C, Francis M, et al. Neuroinflammation, immune system and Alzheimer disease: searching for the missing link. *Aging Clin Exp Res*. 2017;29(5):821–831. doi:10.1007/s40520-016-0637-z

49. Gomaa AA, Makboul RM, Al-Mokhtar MA, Nicola MA. Polyphenol-rich boswellia serrata gum prevents cognitive impairment and insulin resistance of diabetic rats through inhibition of GSK3beta activity, oxidative stress and pro-inflammatory cytokines. *Biomed Pharmacother.* 2019;109:281–292. doi:10.1016/j.biopha.2018.10.056

50. Zhao F, Zhang J, Chang N. Epigenetic modification of Nrf2 by sulforaphane increases the antioxidative and anti-inflammatory capacity in a cellular model of Alzheimer's disease. *Eur J Pharmacol.* 2018;824:1–10. doi:10.1016/j.ejphar.2018.01.046

51. Mancini S, Balducci C, Micotti E, et al. Multifunctional liposomes delay phenotype progression and prevent memory impairment in a presymptomatic stage mouse model of Alzheimer disease. *J Control Release.* 2017;258:121–129. doi:10.1016/j.jconrel.2017.05.013

52. Xiao S, Zhou D, Luan P, et al. Graphene quantum dots conjugated neuroprotective peptide improve learning and memory capability. *Biomater.* 2016;106:98–110. doi:10.1016/j.biomaterials.2016.08.021

53. Guo Q, Zheng X, Yang P, et al. Small interfering RNA delivery to the neurons near the amyloid plaques for improved treatment of Alzheimers disease. *Acta Pharm Sin B.* 2019;9(3):590–603. doi:10.1016/j.apsb.2018.12.010

54. Sharma A. Liposomes in drug delivery: progress and limitations. *Int J Pharm.* 1997;154(2):123–140. doi:10.1016/S0378-5173(97) 00135-X

55. Bozzuto G, Molinari A. Liposomes as nanomedical devices. *Int J Nanomedicine.* 2015;10:975–999. doi:10.2147/IJN.S68861